

# RSC Advances



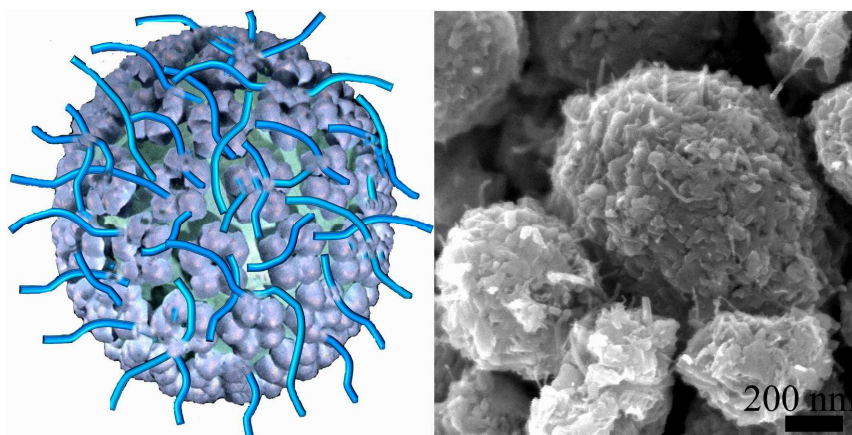
This is an *Accepted Manuscript*, which has been through the Royal Society of Chemistry peer review process and has been accepted for publication.

*Accepted Manuscripts* are published online shortly after acceptance, before technical editing, formatting and proof reading. Using this free service, authors can make their results available to the community, in citable form, before we publish the edited article. This *Accepted Manuscript* will be replaced by the edited, formatted and paginated article as soon as this is available.

You can find more information about *Accepted Manuscripts* in the [Information for Authors](#).

Please note that technical editing may introduce minor changes to the text and/or graphics, which may alter content. The journal's standard [Terms & Conditions](#) and the [Ethical guidelines](#) still apply. In no event shall the Royal Society of Chemistry be held responsible for any errors or omissions in this *Accepted Manuscript* or any consequences arising from the use of any information it contains.

## Table of content entry



A three-dimensional nanoarchitecture consisting of mesoporous  $V_2O_5$  and penetrating CNTs was synthesized for high-performance lithium-ion batteries.

## COMMUNICATION

# Carbon nanotube-penetrated mesoporous V<sub>2</sub>O<sub>5</sub> microspheres as a high-performance cathode material for lithium-ion batteries

Xilai Jia,<sup>a,b</sup> Liqiang Zhang,<sup>b</sup> Rufan Zhang,<sup>a</sup> Yunfeng Lu<sup>\*c</sup> and Fei Wei<sup>\*a</sup>

Received (in XXX, XXX) Xth XXXXXXXXX 20XX, Accepted Xth XXXXXXXXX 20XX

DOI: 10.1039/b000000x

**A three-dimensional nanoarchitecture consisting of mesoporous V<sub>2</sub>O<sub>5</sub> and penetrating CNTs was synthesized via aerosol spray drying process followed by two-step thermal anneal. The nanocomposites show hierarchical structure for effective ion and electron transport, making their lithium-ion battery electrodes show superhigh capacity and rate-capability.**

High-performance electrochemical energy storage devices, such as lithium-ion batteries, are of great importance for a broad range of applications.<sup>1</sup> Based on the shuttle of ion and electron transport during their charge and discharge processes, chemical energy and electric energy are reversibly transformed, respectively. However, current battery technologies are mostly limited by such kinetic problems.<sup>2</sup> Vanadium pentoxide (V<sub>2</sub>O<sub>5</sub>) shows high theoretical capacity (~296 mAh g<sup>-1</sup> based on two lithium intercalation) and can be synthesized at low cost, which make it a promising cathode candidate for batteries. However, V<sub>2</sub>O<sub>5</sub> exhibits slow ion diffusion and poor electronic conductivity. The design of the ion and electron transport is thereby the most important consideration for a better performance.

In this context, low-dimensional V<sub>2</sub>O<sub>5</sub> materials such as the nanoparticles,<sup>3</sup> nanowires,<sup>4</sup> nanosheets,<sup>5</sup> nanobelts<sup>6</sup> and nanorods,<sup>7</sup> have been synthesized and attained improved performances, since the low dimensionality has shortened ion diffusion length. However, the use of such low-dimensional V<sub>2</sub>O<sub>5</sub> always leads to undesired problems of loading, interfaces and handing.<sup>2</sup> Based on the low-dimensional building blocks, 3D nanostructured V<sub>2</sub>O<sub>5</sub> architectures have been synthesized, including the nanostructured fibers,<sup>8</sup> arrays,<sup>9</sup> films,<sup>10</sup> microspheres,<sup>11</sup> microflowers<sup>12</sup> and foams.<sup>13</sup> Accordingly, interconnected pore channels for electrolyte transport and shortened ion diffusion length are built in those architectures; however, effective electron transport is still required for further improvement.<sup>14</sup> Nanocarbon materials such as carbon nanotubes (CNTs) and graphene have therefore emerged to replace traditional carbon blacks in battery techniques,<sup>15</sup> since they could offer long-range conductivity, better interfacial contacts, and more robust structure. To date, various approaches (*e.g.*, direct mechanical mixing,<sup>16</sup> *in-situ* hydrothermal growth,<sup>17</sup> sol-gel,<sup>18</sup> atomic layer deposition (ALD),<sup>19</sup> etc.) have been proposed to construct such nanocomposites, such as the commonly mixed “entangled network” nanocomposites with V<sub>2</sub>O<sub>5</sub> entangled with CNTs,<sup>16</sup> and “core-shell”

hybrid nanocomposites with V<sub>2</sub>O<sub>5</sub> coated on CNT surfaces.<sup>20</sup> Nevertheless, those nanocomposites mostly cannot form 3D structures, thus only facilitates charge transfer locally. Some 3D nanocomposites have been fabricated using the ALD technique,<sup>19</sup> such deposition processes, however, require expensive precursors and facilities and is difficult to be implemented for large-scale production.

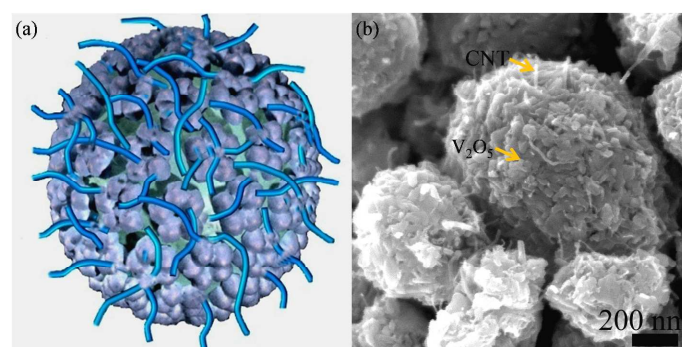


**Fig. 1** (a) Schematic illustration of the structure and (b) SEM image of CNT/V<sub>2</sub>O<sub>5</sub> nanocomposite microspheres.

Herein, we propose the construction of a novel 3D nanoarchitecture using facile aerosol-spray drying process that consists of nanostructured mesoporous V<sub>2</sub>O<sub>5</sub> and penetrating CNTs as high-performance cathode materials (Fig. 1a). In contrast to prior work on V<sub>2</sub>O<sub>5</sub>-based electrodes,<sup>11</sup> our design, firstly, presents two-levels of ion transport in the nanocomposites, including interconnected pore networks for facile electrolyte access and mesoporous structure of V<sub>2</sub>O<sub>5</sub> with shortened ion-diffusion length. Then, CNTs are directly assembled into V<sub>2</sub>O<sub>5</sub> for efficient electron transport. Moreover, the structured pores of the nanocomposites is able to accommodate the volume changes during lithium insertion/extraction process, desired for cycling stability. Therefore, the nanocomposites simultaneously achieve robust ion and electron transport, and are expected to produce high-performance batteries.

To fabricate the nanocomposites, we started with dispersing CNTs into a precursor solution of V<sub>2</sub>O<sub>5</sub>, forming a homogeneous dispersion. Simultaneously, a surfactant (F127, polyethylene glycol, propoxylated) was also introduced into the dispersion for templating. The atomization process using nitrogen as the carrier gas

## COMMUNICATION

continuously generated precursor droplets containing CNTs. After passing through a heated tube furnace, solvent evaporation of the droplets enriched the precursor and condensed CNTs into the solid particles. Subsequent two-step thermal treatments using hydrogen and air annealing in sequence converted the collected particles into the final CNT/V<sub>2</sub>O<sub>5</sub> nanocomposite microspheres (Fig. 1b), which are made from networks of V<sub>2</sub>O<sub>5</sub> and penetrating CNTs throughout the microspheres.

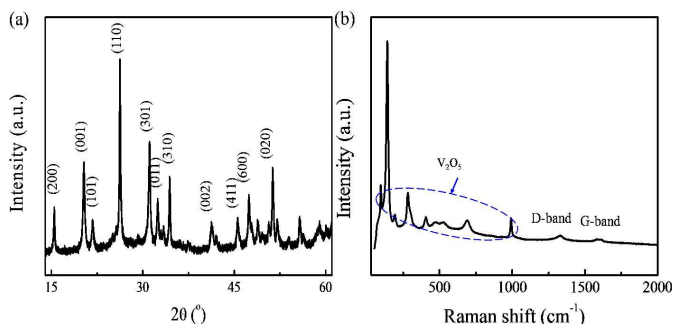


**Fig. 2** (a) XRD pattern and (b) Raman spectrum of CNT/V<sub>2</sub>O<sub>5</sub> nanocomposite microspheres.

The morphology and structure of the nanocomposites was first investigated using X-ray diffraction (XRD), Raman spectroscopy and electron microscopic techniques. Fig. 2a shows the XRD pattern of the nanocomposites. It exhibited intense diffraction peaks of orthorhombic V<sub>2</sub>O<sub>5</sub> phase (space group *Pmmn*, JCPDS card No. 41-1426), suggesting a successful transformation of the V-precursor into V<sub>2</sub>O<sub>5</sub>. Note that the characteristic CNT diffraction peak at 26.2° was not visible; however, Raman spectrum (Fig. 2b) of the nanocomposites detected carbon peaks with characteristic disorder-induced D and graphitic G bands at 1336 and 1582 cm<sup>-1</sup>, respectively. The results suggest two phases, namely V<sub>2</sub>O<sub>5</sub> and carbon, coexist in the nanocomposites. The elemental mapping of the nanocomposites was obtained by energy dispersive X-ray spectroscopy (EDX, Fig. S1), which confirmed their distributions. The chemical composition was further determined by thermogravimetric analysis as displayed in Fig. S2, which was composed of 94 wt-% V<sub>2</sub>O<sub>5</sub> and 6 wt-% carbon components.

Scanning electron microscopic (SEM) image shows that the nanocomposite microspheres are spherical in shape with polydisperse submicron sizes (Fig. S3). Such nanocomposites can circumvent the limitation of nanoparticles and offer easier handling in actual production.<sup>2</sup> It is worth mentioning that direct thermal treatment of the collected spray-dried particles at 400 °C in air has failed to obtain the nanocomposites, because the nanostructured microspherical morphologies are destroyed in a certain degree and the CNTs are completely oxidized as indicated by Fig. S4. The thermal treatment at a lower temperature such as 300 °C in air, however, cannot fully achieve the formation of V<sub>2</sub>O<sub>5</sub> (Fig. S5). Note that some CNT/V<sub>2</sub>O<sub>5</sub> nanocomposites have been obtained under treatment at 400 °C in air;<sup>21</sup> it could be ascribed to the nanotubes used and the structure properties of the nanocomposites.

Transmission electron microscopic (TEM, Fig. 3a) image further confirms the interconnected 3D networks of the nanocomposites. Close TEM observation (Fig. 3b) shows the direct

interfacial contacts between CNTs and active materials. As expected, CNTs were assembled into V<sub>2</sub>O<sub>5</sub> with no phase separation. Such direct interfacial contacts facilitate effective electron transport, a key factor affecting the electrode's rate performance. In comparison, direct mechanical-mixing nanocomposites<sup>16</sup> and recently developed interpenetrating nanocomposites<sup>22</sup> can hardly provide such intimate interfacial contacts. TEM observation further reveals the mesoporous structure of V<sub>2</sub>O<sub>5</sub> (Fig. 3c). It displayed that V<sub>2</sub>O<sub>5</sub> had abundant mesopores of 2-4 nm, which should be produced from the decomposition of the surfactant. Those distributed mesopores serve as electrolyte storage points for locally efficient ion transport. Moreover, Fig. 3c suggests V<sub>2</sub>O<sub>5</sub> microspheres are composed of a layered crystalline structure with a layer-to-layer distance of ~ 2.1 Å, which can accommodate facile ion transport. Selected area electron diffraction (SAED, inset of Fig. 3c) further reveals their polycrystalline nature.

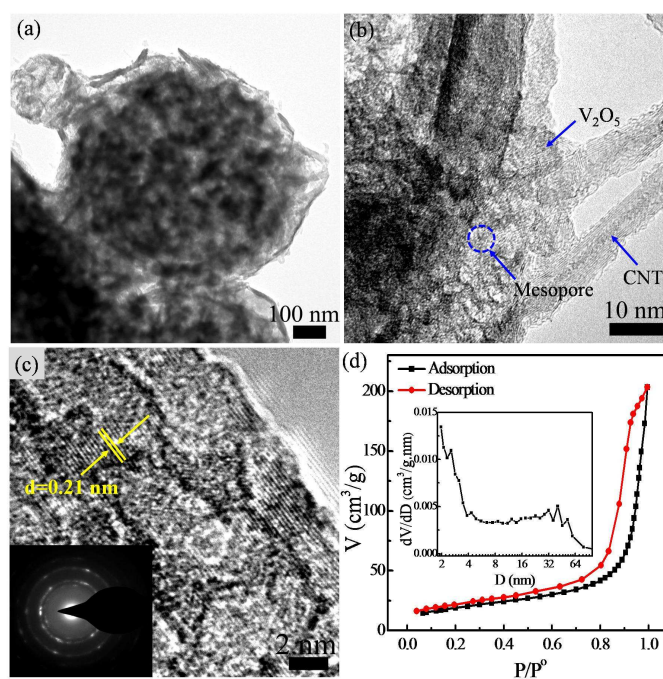


**Fig. 3** (a-c) TEM images of CNT/V<sub>2</sub>O<sub>5</sub> nanocomposite microspheres. (d) Nitrogen isotherms of the nanocomposite microspheres.

Their 3D structure of CNT/V<sub>2</sub>O<sub>5</sub> nanocomposites was further confirmed using nitrogen adsorption measurement (Fig. 3d). It exhibited a high Brunauer–Emmett–Teller (BET) surface area of 95.8 m<sup>2</sup> g<sup>-1</sup>. Significant nitrogen uptake at a high relative pressure of nitrogen, as well as the absence of adsorption-desorption hysteresis, suggests the formation of interconnected porous channels. Nitrogen adsorption-desorption isotherms also suggest that the nanocomposites exhibit hierarchically structured pores with a broad pore size distribution ranging from several nanometers to nearly one hundred nanometers (inset of Fig. 3d). More specifically, the continuous pore channels around 4-60 nm could be summarily ascribed to the interconnected pores; while the abundant mesopores below 4 nm should be rooted from mesopores of V<sub>2</sub>O<sub>5</sub>. In short, based on the structure characterizations, it is convincing that the

## RSC Advances

designed nanocomposite microspheres are effective for ion and electron transport.

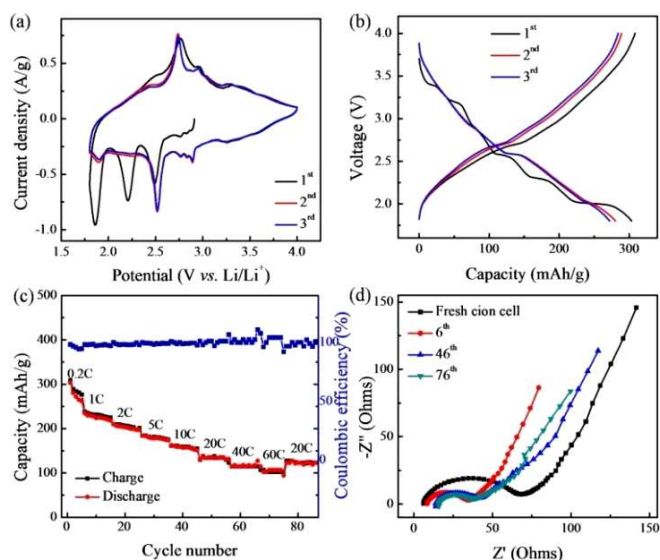


**Fig. 4** (a) The first three CV curves of the nanocomposite electrode at  $0.5 \text{ mV s}^{-1}$  and (b) the galvanostatic charge/discharge curves cycled at a current density of  $50 \text{ mA g}^{-1}$  between voltage limits of  $1.8\text{--}4.0 \text{ V}$ . (c) Rate performance and cycling stability of the nanocomposite electrode. (d) Nyquist plots of the nanocomposite electrode at different cycling stages.

The cathode performance of CNT/ $\text{V}_2\text{O}_5$  nanocomposites was shown in Fig. 4. Charge storage behaviour was characterized by cyclic voltammetry (CV, Fig. 4a). The electrochemical  $\text{Li}^+$  insertion/extraction process can be expressed by  $\text{V}_2\text{O}_5 + x \text{Li}^+ + x \text{e}^- \leftrightarrow \text{Li}_x\text{V}_2\text{O}_5$ , where  $x$  is the mole fraction of inserted Li ions. For the first cathodic scan, multiple reduction peaks located at  $2.9$ ,  $2.5$ ,  $2.2$ ,  $1.9 \text{ V}$  are observed due to the phase transformations associated with Li insertion, which give  $\epsilon\text{-Li}_x\text{V}_2\text{O}_5$ ,  $\delta\text{-Li}_x\text{V}_2\text{O}_5$ ,  $\omega\text{-Li}_x\text{V}_2\text{O}_5$ , and  $\gamma\text{-Li}_x\text{V}_2\text{O}_5$ , respectively.<sup>23</sup> Note that the formation of  $\omega\text{-Li}_x\text{V}_2\text{O}_5$  and  $\gamma\text{-Li}_x\text{V}_2\text{O}_5$  phases is irreversible due to the deep Li insertion. However, following cycles are highly reversible, suggesting facile phase transformations at the nanoscale. Consistent with the CV curves, charge/discharge curves at a current density of  $50 \text{ mA g}^{-1}$  displayed that the first charge and discharge capacity based on the total mass of electrode was  $308$  and  $303 \text{ mAh g}^{-1}$ , respectively (Fig. 4b). It corresponds to an initial coulombic efficiency of  $98 \%$ , which is extremely high for lithium-ion batteries. When increasing the current densities (Fig. S6a), improved kinetics of Li insertion/extraction was maintained due to the hierarchical structure of the nanocomposites and more importantly, increased conductivity from CNTs. The capacity contribution of CNTs within the nanocomposite electrode was relatively small compared to that of  $\text{V}_2\text{O}_5$  at the voltage of  $1.8\text{--}4.0 \text{ V}$  (Fig. S7). Based on the mass of  $\text{V}_2\text{O}_5$  component, it displayed a discharge capacity of  $\sim 442 \text{ mAh g}^{-1}$  at  $50 \text{ mA g}^{-1}$ , which is markedly higher than those of reported  $\text{V}_2\text{O}_5$ -based cathodes.<sup>24</sup> Obviously, the designed nanocomposites can make the best of active materials.

Fig. 4c shows the rate and cycling performance of CNT/ $\text{V}_2\text{O}_5$  electrode at different current densities. In spite of a capacity decrease of *ca.*  $10 \%$  during the initial cycles that are commonly

observed for V-oxides,<sup>25</sup> the electrode shows stable capacity at various C rates. The total discharge capacity of the electrode reached  $\sim 300 \text{ mAh g}^{-1}$  at  $0.2 \text{ C}$ . Even at high rates of  $20$  and  $60 \text{ C}$ , the electrode still delivered reversible capacity of  $132$  and  $104 \text{ mAh g}^{-1}$ . In comparison, the electrode made from aerosol-synthesized  $\text{V}_2\text{O}_5$  microspheres showed a little lower rate-capability due to the inefficient electron transport (Fig. S6b). Such rate capability is really impressive. Furthermore, upon returning back to the rate of  $20 \text{ C}$  after  $75$  cycles at different rates, the nanocomposite electrode still delivered discharge capacity of  $130 \text{ mAh g}^{-1}$ . Such an electrode still also presents a capacity over  $210 \text{ mAh g}^{-1}$  after  $60$  cycles at the charge/discharge rate of  $0.5 \text{ C}$  (Fig. S8), suggesting a moderate stability. Comparing with several high-rate  $\text{V}_2\text{O}_5$  electrodes of recent work,<sup>21,26</sup> the designed nanocomposite electrode shows comparable or much better performance. Importantly, the performance is based on the total weight of active nanocomposite materials, binders and conductive additives. With the demand for efficient power batteries, there usually is a compromise of the storage capability and discharge rate. Herein, the high energy and power density were combined by such 3D nanostructured composites, making them promising for high-power devices.

Electrochemical impedance spectroscopy (EIS) was carried out to probe the structure properties of the nanocomposite electrode along with cycling. Nyquist plots of the electrode at different cycling status are shown in Fig. 4d. It was found that the fresh electrode exhibited a relatively large single semicircle and an intercept at high frequency range, which was associated with a combination of ohmic and charge-transfer resistance, and a low-frequency Warburg tail associated with ion diffusion resistance. Interestingly, the diameter of the semicircle decreases and the slope of the Warburg tail increases after  $5$  cycles at  $0.2 \text{ C}$ , indicating a decreased charge-transfer resistance and improved lithium-diffusion rate. It may be due to removal of the protons from the electrodes and better CNT- $\text{V}_2\text{O}_5$  interfaces induced by the charge/discharge processes.<sup>22</sup> The impedance behaviour shows similar features during the following cycles, confirming the robust structure of the nanocomposites. Even after  $75$  cycles, the charge transport resistance remains small, and accordingly, the capacity is well maintained with high stability.

In summary, we have demonstrated a novel 3D CNT/ $\text{V}_2\text{O}_5$  nanoarchitecture consisting of hierarchically structured  $\text{V}_2\text{O}_5$  and penetrating CNTs. The nanocomposites are realized by an efficient aerosol spray drying process followed by anneal processes. Due to the nanostructured features, such nanocomposites have effective charge transport, thus offering batteries high capacity and rate-capability performance. The synthesis method may be extended to synthesize other cathode and anode electrode materials for energy storage devices.

This work was supported by National Basic Research Program of China (973 Program, 2011CB932602) and Natural Scientific Foundation of China (No. 21306102), and was partially supported by Science Foundation of China University of Petroleum, Beijing (No. 2462013YJRC028).

<sup>a</sup> Beijing Key Laboratory of Green Chemical Reaction Engineering and Technology, Department of Chemical Engineering, Tsinghua University,

## COMMUNICATION

Beijing 100084, P.R. China. Fax: (+86)10-6277-2051, E-mail: wf-dce@tsinghua.edu.cn

<sup>b</sup> State Key Laboratory of Heavy Oil Processing, China University of Petroleum, Changping, Beijing 102249, P. R. China.

<sup>c</sup> Department of Chemical and Biomolecular Engineering, University of California, Los Angeles, CA 90095. E-mail: luucla@ucla.edu

Electronic Supplementary Information (ESI) available. See DOI: 10.1039/c000000x/

## Notes and references

- C. Liu, F. Li, L. P. Ma, H. M. Cheng, *Adv. Mater.*, 2010, **22**, E28.
- P. G. Bruce, B. Scrosati, J. M. Tarascon, *Angew. Chem. Int. Ed.*, 2008, **47**, 2930.
- X.-F. Zhang, K.-X. Wang, X. Wei, J.-S. Chen, *Chem. Mater.*, 2011, **23**, 5290; M. Koltypin, V. Pol, A. Gedanken, D. Aurbach, *J. Electrochem. Soc.*, 2007, **154**, A605.
- J. W. Lee, S. Y. Lim, H. M. Jeong, T. H. Hwang, J. K. Kang, J. W. Choi, *Energy Environ. Sci.*, 2012, **5**, 9889; H. Liu, W. Yang, *Energy Environ. Sci.* 2011, **4**, 4000.
- Y. Li, J. Yao, E. Uchaker, J. Yang, Y. Huang, M. Zhang, G. Cao, *Adv. Energy Mater.*, 2013, **3**, 1171; X. Rui, Z. Lu, H. Yu, D. Yang, H. H. Hng, T. M. Lim, Q. Yan, *Nanoscale*, 2013, **5**, 556.
- G. Li, S. Pang, L. Jiang, Z. Guo, Z. Zhang, *J. Phys. Chem. B*, 2006, **110**, 9383.
- A. M. Glushenkov, M. F. Hassan, V. I. Stukachev, Z. Guo, H. K. Liu, G. G. Kuvshinov, Y. Chen, *J. Solid State Electrochem.*, 2010, **14**, 1841.
- H. G. Wang, D. L. Ma, Y. Huang, X. B. Zhang, *Chem. Eur. J.*, 2012, **18**, 8987; D. Yu, C. Chen, S. Xie, Y. Liu, K. Park, X. Zhou, Q. Zhang, J. Li, G. Cao, *Energy Environ. Sci.*, 2011, **4**, 858; L. Mai, L. Xu, C. Han, X. Xu, Y. Luo, S. Zhao, Y. Zhao, *Nano Lett.*, 2010, **10**, 4750.
- X. Yu, Z. Lu, G. Zhang, X. Lei, J. Liu, L. Wang, X. Sun, *RSC Adv.*, 2013, **3**, 19937.
- X. Chen, E. Pomerantseva, K. Gregorczyk, R. Ghodssi, G. Rubloff, *RSC Adv.*, 2013, **3**, 4294; X. Chen, E. Pomerantseva, P. Banerjee, K. Gregorczyk, R. Ghodssi, G. Rubloff, *Chem. Mater.*, 2012, **24**, 1255.
- J. Shao, X. Li, Z. Wan, L. Zhang, Y. Ding, L. Zhang, Q. Qu, H. Zheng, *ACS Appl. Mater. Interfaces*, 2013, **5**, 7671; A. Pan, H. B. Wu, L. Yu, X. W. Lou, *Angew. Chem. Int. Ed.*, 2013, **125**, 2282; A. M. Cao, J. S. Hu, H. P. Liang, L. J. Wan, *Angew. Chem. Int. Ed.*, 2005, **44**, 4391; J. Liu, Y. Zhou, J. Wang, Y. Pan, D. Xue, *Chem. Commun.*, 2011, **47**, 10380; H. Pang, P. Cheng, H. Yang, J. Lu, C. X. Guo, G. Ning, C. M. Li, *Chem. Commun.*, 2013, **49**, 1536; S. Wang, S. Li, Y. Sun, X. Feng, C. Chen, *Energy Environ. Sci.*, 2011, **4**, 2854; C. Zhang, Z. Chen, Z. Guo, X. W. D. Lou, *Energy Environ. Sci.*, 2013, **6**, 974.
- A. Pan, H. B. Wu, L. Yu, T. Zhu, X. W. Lou, *ACS Appl. Mater. Interfaces*, 2012, **4**, 3874.
- J. Zhu, L. Cao, Y. Wu, Y. Gong, Z. Liu, H. E. Hoster, Y. Zhang, S. Zhang, S. Yang, Q. Yan, P. M. Ajayan, R. Vajtai, *Nano Lett.*, 2013, **13**, 5408.
- J. Liu, D. Xue, *Nanoscale Res. Lett.*, 2010, **5**, 1525.
- R. Yu, C. Zhang, Q. Meng, Z. Chen, H. Liu, Z. Guo, *ACS Appl. Mater. Interfaces*, 2013, **5**, 12394; X. Chen, H. Zhu, Y.-C. Chen, Y. Shang, A. Cao, L. Hu, G. W. Rubloff, *ACS Nano*, 2012, **6**, 7948; A. Ghosh, E. J. Ra, M. Jin, H. K. Jeong, T. H. Kim, C. Biswas, Y. H. Lee, *Adv. Funct. Mater.*, 2011, **21**, 2541; Z.-L. Wang, D. Xu, Y. Huang, Z. Wu, L.-M. Wang, X.-B. Zhang, *Chem. Commun.*, 2012, **48**, 976; Q. Zhu, Z. Li, S. Huang, X. Zhang, W. Chen, G. S. Zakharova, *Electrochim. Acta*, 2012, **81**, 25; H. Gwon, H.-S. Kim, K. U. Lee, D.-H. Seo, Y. C. Park, Y.-S. Lee, B. T. Ahn, K. Kang, *Energy Environ. Sci.*, 2011, **4**, 1277; W. Tang, X. Gao, Y. Zhu, Y. Yue, Y. Shi, Y. Wu, K. Zhu, *J. Mater. Chem.*, 2012, **22**, 20143; X. Zhou, G. Wu, J. Wu, H. Yang, J. Wang, G. Gao, R. Cai, Q. Yan, *J. Mater. Chem. A*, 2013, **1**, 15459; X. Rui, J. Zhu, D. Sim, C. Xu, Y. Zeng, H. H. Hng, T. M. Lim, Q. Yan, *Nanoscale*, 2011, **3**, 4752; J. S. Sakamoto, B. Dunn, *J. Electrochem. Soc.*, 2002, **149**, A26; W. Lu, A. Goering, L. Qu, L. Dai, *Phys. Chem. Chem. Phys.*, 2012, **14**, 12099; G. Du, K. H. Seng, Z. Guo, J. Liu, W. Li, D. Jia, C. Cook, Z. Liu, H. Liu, *RSC Adv.*, 2011, **1**, 690; S. Li, D. Wu, C. Cheng, J. Wang, F. Zhang, Y. Su and X. Feng, *Angew. Chem.*, 2013, **125**, 12327; V. V. Kulish, M.-F. Ng, O. I. Malyi, P. Wu and Z. Chen, *RSC Adv.*, 2013, **3**, 8446; Y. Su, S. Li, D. Wu, F. Zhang, H. Liang, P. Gao, C. Cheng and X. Feng, *ACS Nano*, 2012, **6**, 8349; C. Cheng, S. Li, J. Zhao, X. Li, Z. Liu, L. Ma, X. Zhang, S. Sun and C. Zhao, *Chem. Eng. J.*, 2013, **228**, 468; T. Chen, L. Pan, X. Liu, K. Yu and Z. Sun, *RSC Adv.*, 2012, **2**, 11719; X. Jia, C. Yan, Z. Chen, R. Wang, Q. Zhang, L. Guo, F. Wei and Y. Lu, *Chem. Commun.*, 2011, **47**, 9669.
- K. H. Seng, J. Liu, Z. P. Guo, Z. X. Chen, D. Jia, H. K. Liu, *Electrochem. Commun.*, 2011, **13**, 383.
- Z. Chen, Y. Qin, D. Weng, Q. Xiao, Y. Peng, X. Wang, H. Li, F. Wei, Y. Lu, *Adv. Funct. Mater.*, 2009, **19**, 3420.
- S. Liang, M. Qin, J. Liu, Q. Zhang, T. Chen, Y. Tang, W. Wang, *Mater. Lett.*, 2013, **93**, 435.
- S. Boukhalfa, K. Evanoff, G. Yushin, *Energy Environ. Sci.*, 2012, **5**, 6872.
- M. Sathiy, A. S. Prakash, K. Ramesha, J. M. Tarascon, A. K. Shukla, *J. Am. Chem. Soc.*, 2011, **133**, 16291.
- Y. S. Hu, X. Liu, J. O. Müller, R. Schlögl, J. Maier, D. S. Su, *Angew. Chem. Int. Ed.*, 2009, **48**, 210.
- X. Jia, Z. Chen, A. Suwarnasarn, L. Rice, X. Wang, H. Sohn, Q. Zhang, B. M. Wu, F. Wei, Y. Lu, *Energy Environ. Sci.*, 2012, **5**, 6845.
- C. K. Chan, H. Peng, R. D. Twisten, K. Jarausch, X. F. Zhang, Y. Cui, *Nano Lett.*, 2007, **7**, 490; J. Liu, H. Xia, D. Xue, L. Lu, *J. Am. Chem. Soc.* 2009, **131**, 12086.
- T. Zhai, H. Liu, H. Li, X. Fang, M. Liao, L. Li, H. Zhou, Y. Koide, Y. Bando, D. Golberg, *Adv. Mater.*, 2010, **22**, 2547; S. Wang, Z. Lu, D. Wang, C. Li, C. Chen, Y. Yin, *J. Mater. Chem.*, 2011, **21**, 6365.
- Z. Cao, B. Wei, *Nano Energy*, 2013, **2**, 481; F. Carn, M. Morcrette, B. Desport, R. Backov, *Solid State Sci.*, 2013, **17**, 134.
- H. Yamada, K. Tagawa, M. Komatsu, I. Moriguchi, T. Kudo, *J. Phys. Chem. C*, 2007, **111**, 8397; A. Pan, J.-G. Zhang, Z. Nie, G. Cao, B. W. Arey, G. Li, S.-Q. Liang, J. Liu, *J. Mater. Chem.*, 2010, **20**, 9193.